



Plagiarism Checker X Originality Report

Similarity Found: 23%

Date: Monday, April 27, 2020

Statistics: 1073 words Plagiarized / 4595 Total words

Remarks: Medium Plagiarism Detected - Your Document needs Selective Improvement.

Bull. **Mater. Sci. (2020) 43:11** © Indian Academy of Sciences
<https://doi.org/10.1007/s12034-019-1984-0> High-temperature corrosion of
aluminized-AISI 1020 steel with NaCl and Na₂SO₄ deposits M BADARUDDIN 1,* ,
SUGIYANTO 1 and D A SMI 2 1Department of Mechanical Engineering, Faculty of
Engineering, Universitas Lampung, Bandar Lampung 35145, Indonesia 2Department of
Physics, Faculty of Mathematics and Natural Science, Universitas Lampung, Bandar
Lampung 35145, Indonesia *Author for correspondence (mbruddin@eng.unila.ac.id) MS
received 27 August 2018; accepted 10 July 2019 Abstract.

High-temperature corrosion of aluminized-American Iron and Steel Institute (AISI) 1020
steel with sodium chloride (NaCl) and sodium sulphate (Na₂SO₄) deposits was studied
using isothermal oxidation in a dry air environment at 700°C for 49 h. NaCl and
Na₂SO₄ deposits on the aluminide layer interfered with protective alumina/aluminium
oxide (Al₂O₃) scale formation on the steel substrate.

Chlorine and sulphur gases (Cl₂g and S_g, respectively) released into the atmosphere
corroded the protective Al₂O₃ layer. Corrosion of the Al₂O₃ layer was also due to local
formation of iron oxide (Fe₂O₃). Fe₂O₃ growth is attributed to ferric chloride (FeCl₃)
vaporization. S_g diffusion into the Al₂O₃ scale via Al³⁺ vacancy defects led to the
formation of aluminium sulphide on the aluminide layer surface.

Cl and S consequently induced hot corrosion of the aluminized steel, thereby increasing
cyclic oxychloridation and sulphidation rates at high temperatures. Keywords.
Aluminized 1020 steel; hot corrosion; oxychloridation; sulphidation; alumina/aluminium
oxide (Al₂O₃). 1. Introduction Cold-rolled American Iron and Steel Institute (AISI) 1020
steel is a material suitable for engineering components because of its relatively low cost

compared with that of high-alloy steel.

This steel is used in heat exchangers, oil gas tanks, high-pressure water pipes and other equipment for fossil fuel power plants. Alkali metal sulphates produced by low-grade fuel combustion react with sodium chloride (NaCl) from ocean breezes at elevated temperatures, forming sodium sulphate (Na₂SO₄), which severely corrodes the material by oxidation, sulphidation or chloridation, thus rendering it prone to hot corrosion [1–3].

Therefore, the presence of NaCl and Na₂SO₄ deposits on engineering material components at high temperatures causes rapid degradation of the material [4,5]. In this regard, hot-dipped aluminide steel has great potential in engineering components for harsh environments. Several studies have reported that the aluminium (Al) coating and its alloys can improve carbon steel resistance to oxidation at high temperatures [6–8].

The aluminide layer on steel can supply Al atoms and form a protective aluminium oxide (Al₂O₃) layer. To widen the application range and service life of aluminide steel, hot-corrosion behaviour and its related mechanism must be characterized. Therefore, we studied the effects of NaCl and Na₂SO₄ deposits on the surfaces of aluminized and bare steel (AS and BS) by isothermally oxidizing them at 700°C for 49 h in a static-air environment. The corrosion kinetics was analysed to determine the parabolic rate constant of corrosion (k_p).

Oxidized AS samples were characterized by both optical and scanning electron microscopy (OM and SEM, respectively), energy dispersive X-ray spectroscopy (EDS) and X-ray diffraction (XRD) to determine the possible corrosion causing mechanisms. 2. Experimental 2.1 Specimen preparation A commercial cold-rolled AISI 1020 steel plate with a chemical composition of 0.2C–0.05P–0.05S–0.5Mn (wt%; iron [Fe]-balanced) was cut into specimens with dimensions of 20×10×2mm³.

Before Al deposition, all specimens were ultrasonically cleaned with a solution of 5% sodium hydroxide (NaOH) and 10% phosphoric acid (H₃PO₄) and then covered with Al welding flux pasta. Commercial Al–0.5 wt% silicon (Si) was melted in an alumina (Al₂O₃) crucible at 700°C, and the specimens were then dipped for 16 s in a molten Al bath.

After the aluminizing process, oxide flux deposited on the surface of the aluminized specimens was 0123456789().: V,-vol 11 Page 2 of 8 Bull. Mater. Sci. (2020) 43:11 Figure 1. SEM and EDS results: (a) cross-sectional micrograph and (b) iron (Fe) and aluminium (Al) element line-scan results for aluminized AISI 1020 steel.

cleaned with a solution of nitric acid, H₃PO₄ and water (1:1:1, v/v) at room temperature. 2.2 Corrosion testing and characterization of samples A saturated NaCl and Na₂SO₄ solution was sprayed onto the largest surface of each specimen placed on a 200°C hot plate to form deposits at a concentration of 2 mg cm⁻². As a result of NaCl and Na₂SO₄ at a concentration of 2 mg cm⁻² was similar to that reported in the literature [9,10].

All BS and AS specimens with NaCl and Na₂SO₄ coatings were isothermally oxidized at 700°C for 1–49 h. In the present investigation, a temperature of around 700°C is referred to as type-II hot corrosion, which occurs at temperatures below that of salt melting [11]. After a given isothermal oxidation time, the specimens were removed and cooled in air at room temperature.

Each data point for corrosion kinetic-related weight gain was obtained from a different specimen. Linear and parabolic plots of the weight gain (mg cm⁻²) vs. oxidation time (h) were constructed. The aluminide layer thickness and microstructures of aluminized specimens were observed by OM. The phases formed on steel were identified by XRD using monochromatic Cu K α radiation at 40 kV and 100 mA.

The surface and cross-sectional morphologies of AS were examined by SEM and EDS, respectively. 3. Results and discussion 3.1 Examination of the coated specimen An SEM cross-sectional micrograph and EDS element line scan for the aluminide coating and the steel substrate after the aluminizing process are displayed in Figure 1a and b, respectively.

When low-carbon steel and molten Al came into contact with each other during the hot-dipping process, a thin intermetallic compound (IMC) formed between the steel and aluminide layer. However, not all of the IMCs formed during the aluminizing hot-dip coating, except for the Fe₂Al₅ and FeAl₃ phases, could be confirmed [12]. The formation of the IMCs in the Al-rich zone suggests that inward diffusion of Fe and outward diffusion of Al predominantly controlled the phase transformation and formed an aluminide layer on the steel substrate.

The thickness of the aluminide layer consisting of the Al and FeAl₃/Fe₂Al₅ intermetallic layers was about 50 μm (FeAl₃: 5.403 μm and Fe₂Al₅: 17.401 μm). This coating layer showed no cracks and voids at the interface between the aluminide layer and steel substrate. In addition, an EDS element line scanning showed that the Fe content of the Al coating was much less than that of the intermetallic layer.

This may have been caused by the lower diffusion rate of Fe atoms in molten Al compared with that of Al atoms in Fe [13]. The Al content decreased while the FeAl₃ and

Fe₂Al₅ content increased towards the steel sub- strate after formation of the aluminizing coating by the hot-dip process (Figure 1b). 3.2 Corrosion kinetics Figure 2a shows the corrosion kinetics of AS after oxidation at 700°C for 49 h in various environments.

Corresponding data for BS are also included for comparison. As seen in Figure 2a, BS showed a rapid weight gain for up to 49 h. As weight gain caused by NaCl deposits was slow during the initial corrosion stage (up to 9 h; 2.5 mg cm⁻²), the rate gradually decreased to 2.1 mg cm⁻² after 49 h of corrosion. Similarly, AS with Na₂SO₄ deposits showed a slow weight gain at 1.4 mg cm⁻² after 49 h of corrosion.

AS showed weight gains lower than those of AS specimens with NaCl and Na₂SO₄ deposits oxidized at 700°C in dry air. Bull. Mater. Sci. (2020) 43:11 Page 3 of 8 11 Figure 2. Corrosion kinetics of BS and aluminized AISI 1020 steel at 700°C: (a) linear plot at 49 h and (b) parabolic plot at 9 h. Pieraggi [14] suggested that plots of a weight gain (ΔW) vs.

$t^{1/2}$ may be a more useful and accurate analysis for the real effect on the oxidation kinetics of pure metals due to primary oxide scale growth. Therefore, plots of weight gain and square roots of time for all specimens undergoing oxidation for 9 h in the parabolic regime are displayed in Figure 2b, and the parabolic rate constant (k_p) was determined by linear regression. The k_p values for BS with NaCl and Na₂SO₄ deposits were 3.721×10^{-9} and 4.122×10^{-9} g² cm⁻⁴ s⁻¹, respectively; the k_p value for BS without NaCl or Na₂SO₄ deposits oxidized in dry air was 2.735×10^{-9} g² cm⁻⁴ s⁻¹.

The k_p values for AS with NaCl and Na₂SO₄ deposits were 1.082×10^{-10} and 3.204×10^{-12} g² cm⁻⁴ s⁻¹, respectively, and that for AS in dry air was 7.517×10^{-13} g² cm⁻⁴ s⁻¹. According to the k_p values, the aluminide layer on AISI 1020 steel appears to play an important role in forming a protective alumina/aluminium oxide (Al₂O₃) scale [8,15]. Consequently, k_p values for AS with NaCl and Na₂SO₄ coatings decreased by one and three orders of magnitude, respectively.

These reductions are attributed to the growth of an Al₂O₃ layer, which led to the establishment of a barrier at the Al₂O₃/aluminide layer interface [16]. The oxidation rates for AS with NaCl and Na₂SO₄ deposits were three and one order(s), respectively, of magnitude higher than those of AS in dry air (Figure 2b). This enhancement is attributed to the presence of gaseous chlorine (Cl₂g) and sulphur (S_g) from NaCl and Na₂SO₄ decomposition [1,5,7,17,18] via the metal-oxide reaction with Cl and S particles, which led to an active corrosion phenomenon at the Al₂O₃/aluminide coating interface.

The weight gain of AS containing NaCl deposits decreased slowly at oxidation times ranging from 9 to 49 h. This slow decrease may have been due to disruption of Al₂O₃ scale growth by Cl via cyclic oxychloridation, which forms volatile metal chlorides [7,9,19].

3.3 Hot-corrosion mechanisms in AS

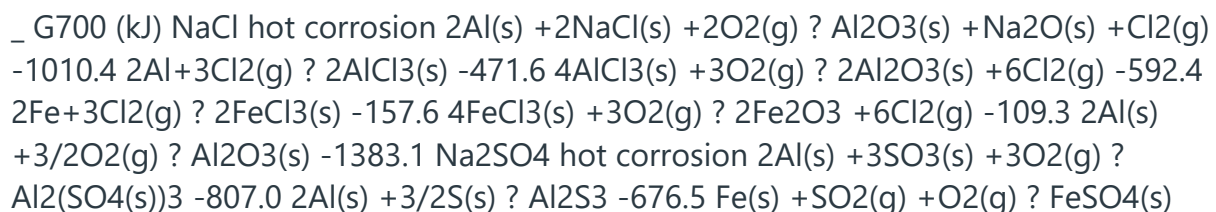
To elucidate the hot-corrosion behaviour and phase transformation in the aluminide layer, saturated NaCl and Na₂SO₄ solutions were deposited on AS specimen surfaces, which were then isothermally oxidized at 700°C for 1–49 h.

In the present study, we speculated that during the initial stages of oxidation, the kinetics was controlled by oxidation of the aluminide coating with oxygen to form Al₂O₃. In further stages of oxidation, hot corrosion occurs in which Al₂O₃ later reacts with the salt deposits and forms a mixture of salts having a lower-melting point than the original salts. The melting points of NaCl and Na₂SO₄ salts were 801 and 884°C [20], respectively.

The NaCl hot-corrosion mechanisms at a 700°C appeared to be similar to those reported by Ciszak et al [18] and Godlewska et al [21]. Furthermore, the Na₂SO₄ hot-corrosion mechanisms at 700°C appear to be similar to those reported by Shi [17] and Yan et al [19]. Thermodynamic data for the reaction kinetics of Fe and Al in the formation of metal chlorides and sulphates were determined based on Gibbs free energy change (ΔG) calculations [22]. ΔG values at 700°C are tabulated in table 1.

Table 1 shows a detailed summary of the possible chemical reactions for accelerating hot-corrosion processes of aluminide layers with NaCl and Na₂SO₄ deposits. The cross-sectional morphologies of AS specimens with NaCl deposits hot corroded at 700°C for 1, 9 and 25 h are presented in figure 3. After 1 h of oxidation, an Fe₂Al₅/FeAl₂ layer and a thin FeAl layer formed on the steel substrate (figure 3a).

The thickness of the aluminide layer depended on the diffusional processing at high temperatures between Al atoms from the aluminide coating and Fe atoms from the steel substrate [13], in which the diffusion coefficient of Fe into Al was $53 \times 10^{-4} \text{ m}^2 \text{ s}^{-1}$ (520–650°C) [23], which was larger than that of Al into Fe, $1.8 \times 10^{-4} \text{ m}^2 \text{ s}^{-1}$ (730–1400°C) [24].



-275.6

$\text{FeSO}_4 \cdot \frac{1}{2}\text{Fe}_2\text{O}_3(\text{s}) + \text{SO}_2(\text{g}) + \frac{1}{4}\text{O}_2(\text{g}) \rightarrow \frac{1}{2}\text{SO}_2(\text{g}) + \frac{1}{2}\text{O}_2(\text{g}) + \text{SO}_3(\text{g})$ -7.6 Figure 3. OM cross-sectional micrographs of AS with NaCl deposits oxidized at 700°C for (a) 1 h, (b) 9 h and (c) 25 h. Therefore, the thickness of an aluminide layer was 162 μm and consisted of Fe₂Al₅, FeAl₂ and FeAl layers and a thin Al₂O₃ scale (Figure 3a).

In addition, some voids could be observed in the outer part of the aluminide layer (Figure 3a) as a result of outward diffusion of Al atoms to form the Al₂O₃ scale, which presented thin and dense characteristics and consisted of an adherent Al₂O₃ layer on the aluminide layer. As the oxidation time increased to 9 and 25 h, the thickness of the Fe₂Al₅/FeAl₂ intermetallic layer decreased due to hot-corrosion attack in the aluminide coating (Figure 3b and c). Some coarse voids and cavities formed in the outer part were filled with a mixture of oxides beneath the Al₂O₃ scale as shown in Figure 3b and c.

XRD examination indicated that identical intermetallic phases (Fe₂Al₅, FeAl₂ and FeAl) formed in the aluminide layer after oxidation of the AS specimens containing NaCl and Na₂SO₄ at 700°C during oxidation progress in an air atmosphere (Figure 4). Bull. Mater. Sci. (2020) 43:11 Page 5 of 8 11 Figure 4. XRD patterns of AS specimens oxidized at 700°C for 9 h in three different environments.

As oxidation time increased, void formation due to outward/inward Al transport predominantly formed pores in the outer part and in the aluminide layer, which is known as the Kirkendall effect [25]. Later, an interconnection of coalescing pores generated crack paths and allowed oxygen (O), Cl₂g and S_g penetration into the aluminide layer, forming the internal oxides (Figure 3b and c). The protective Al₂O₃ layer formed during the early stages could protect the aluminide layer that was directly in contact with NaCl.

However, after 25 h of corrosion, the Fe₂Al₅/FeAl₂ layer was severely degraded (Figure 3c). This result implies that the NaCl deposit plays an important role in the hot-corrosion behaviour of the aluminide layer over long periods. Figure 4 displays the XRD results for the AS with and without NaCl and Na₂SO₄ salt deposits, which confirmed the presence of the oxidation product, Al₂O₃ scale, together with some iron oxide (Fe₂O₃) scales.

The low-intensity diffraction peaks of Al₂O₃ seen in the XRD spectrum in Figure 4 were due to the thin Al₂O₃ scale on the AS specimens oxidized in air. The intensities of Al₂O₃ and Fe₂O₃ peaks for AS specimens with NaCl and Na₂SO₄ deposits increased, indicating that the corrosion layer thickened. It may be argued that Fe₂Al₅, FeAl₂ and FeAl can behave as Al reservoirs that maintain the growth of the Al₂O₃ scale during

long-term oxidation.

As mentioned above, some pores became interconnected and resulted in crack features in which oxidant and corrosive gases consisting of $O_2(g)$, $Cl_2(g)$ and sulphur trioxide ($SO_3(g)$) penetrated into the aluminide layer through the pores and crack paths [25]. The relative decrease in weight gains of the NaCl-deposited AS specimens during a longer oxidation time (9 h) of exposure is believed to be caused by reactions involving metal, NaCl and O, which prevented the formation of a protective oxide scale.

As reported by Cizak et al [18], $Cl_2(g)$ is the first major gaseous species that forms during the reaction of Na-titanium (Ti) oxides at $560^\circ C$. In the present study, the Al_2O_3 formed during the early stage could further react with NaCl and O in the gas atmosphere according to the following reaction [21]: $2NaCl + Al_2O_3 + 1/2O_2 \rightarrow 2NaAlO_2 + Cl_2$ (1) $Cl_2(g)$ was generated by the reaction among Al_2O_3 , NaCl (s) and $O_2(g)$ in which Na-Al oxides that readily penetrated the $Fe_2Al_5/FeAl_2$ layer through crack paths generated during oxidation were also formed.

The $Cl_2(g)$ caused corrosion of the aluminide layer, thereby forming the metal chlorides, ferric chloride ($FeCl_3$) and $AlCl_3$. Both Fe and Al were the driving forces behind metal-chloride formation in the aluminide layer during the initial stages of the reaction [7]. Furthermore, Fe and Al could have dissolved in the molten salt and volatilized or reacted with O.

The melting points of $AlCl_3$ and $FeCl_3$ were 182 and $304^\circ C$, respectively [20], and their thermodynamic equilibrium Gibbs free energies at $700^\circ C$ (ΔG_{700}) were about -471.6 and -157.6 kJ (table 1), respectively. The negative values of ΔG_{700} for the metal chlorides suggest that degradation of the aluminide layer was caused by the formation of Fe and Al chlorides, which are similar findings to those reported by Liu et al [7] and Tsaur et al [25].

In addition, $FeCl_3$ formation was dependent on the activity of Al atoms in the aluminide layer, in which they reach lower concentrations because of their inward diffusion into the steel substrate. Metal chlorides resulted from the reaction of both Al and Fe atoms with $Cl_2(g)$ at $700^\circ C$ in the aluminide layer, thereby increasing the partial pressure of metal chlorides and forcing $AlCl_3$ and $FeCl_3$ to move towards O at high-partial pressures [7].

At the same time, Fe atoms in Fe_2Al_5 and $FeAl_2$ diffused outwards and reacted with Cl to form $FeCl_3$. Subsequently, $FeCl_3$ moved towards O at high-partial pressure, reacting again with O to form Fe_2O_3 . These results are observed in the XRD scan and the

SEM/EDS elemental maps (figures 4 and 5a, respectively).

SEM observation and EDS elemental mapping of the aluminide layer (figure 5a) clearly show that Cl₂g resulted from oxychloridation, which destroyed the protective Al₂O₃ scale on the aluminide layer [15]. Almost all of the Fe₂O₃ scales formed on the FeAl layer, and only a small portion of FeAl₂ remained in the aluminide layer. Fe₂O₃ and Al₂O₃ formed together above the FeAl layer as shown in figure 5a. The Al₂O₃ scale that grew was loose. During oxidation for 11

Page 6 of 8 Bull. Mater. Sci. (2020) 43:11 Figure 5. SEM and EDS elemental maps of AS specimens with (a) NaCl deposits and (b) Na₂SO₄ deposits, oxidized at 700°C for 49 h. 49 h, the FeAl layer replaced the Fe₂Al₅ and FeAl₂ layers, supplying Al atoms that formed the protective Al₂O₃ scale. Furthermore, the presence of Na₂SO₄ deposits on the AS specimens oxidized at 700°C for 49 h had a considerable effect on the corrosion kinetics when compared with AS specimens oxidized in dry air (figure 1a).

In the present study, the experimental temperature was lower than the melting point of Na₂SO₄ (884°C) [20], and the increase in weight gain was about 3.5 times that of AS oxidized in dry air (figure 1a). XRD measurements (figure 4) showed that the intermetallic phases that formed Fe₂Al₅, FeAl₂ and FeAl were the same in various environments.

In addition, Al₂O₃ formed during the early stages of oxidation acted as a barrier to S_g, which could penetrate the aluminide layer in the reaction over short periods. Na₂SO₄ remained on the specimen surface after corrosion testing (figure 4). As reported by Shi [17], accelerated oxidation of Fe with Na₂SO₄ deposits at 750°C may be attributed to a Na₂O/Na₂SO₄ eutectic-melt formation on the surface of the specimen. The salt decomposes when the local partial pressure of O in the environment is lower than that at equilibrium with the Na₂O/Na₂SO₄ eutectic mixture [26].

The partial pressure of O decreased because of O consumption during Al₂O₃ formation in the early stages. When the Na₂SO₄ salt that is deposited on the surface of the specimens does not melt, the following reaction tends to occur on the alumina scale [19]: Na₂SO₄ → Na₂O + SO₂ + 1/2 O₂ (2) Subsequently, the formed Na₂O(s) dissolved in Na₂SO₄, reaching equilibrium with the Na₂O/Na₂SO₄ eutectic mixture [17].

The lower temperature of the eutectic mixture (550°C) [17] is strongly believed to support the formation of aluminium sulphide (Al₂S₃) in the aluminide layer by allowing the release of SO₃g into the atmosphere. Because Na₂SO₄ was still found on the aluminide layer surface after it was oxidized for 9 h (figure 4), the decomposition is believed to supply S that forms Al₂S₃ on the Fe₂Al₅/FeAl₂ layer.

Examination of the SEM cross-sectional micrographs and EDS elemental maps of O, Fe, Al, Cl and S clearly shows a difference between the effects of NaCl [15] and Na₂SO₄ deposits on AS with respect to acceleration of oxidation and corrosion (Figure 5a and b). The micrograph of the corroded sample clearly shows that the aluminide Fe₂Al₅/FeAl₂ layer formed on the FeAl layer (Figure 5b).

Elemental mapping of this scale (Figure 5b) suggests that the corrosion products consisted mainly of Al₂O₃ and some Fe₂O₃ scales. In the early stage of corrosion, an Al₂O₃ scale was quickly formed by unmelted Na₂SO₄ on the surface of the specimens. Bull. Mater. Sci. (2020) 43:11 Page 7 of 8 11 Figure 6.

SEM images of the surface morphologies of AS oxidized at 700°C for 49 h (a) in dry air, (b) in an NaCl environment and (c) in a Na₂SO₄ environment. SEM observation of the AS surface after oxidation in dry air at 700°C for 49 h (Figure 6a) indicates that the Al₂O₃ scale on the aluminide coating is compact. In contrast, Fe₂O₃ and Al₂O₃ grew together on AS with NaCl deposits (Figure 6b).

Furthermore, EDS analysis of the oxide scale (Figure 6c) indicated that a sulphur concentration of 10.02 wt% was sufficient to increase the high ratio of the partial pressure of S_g to the partial pressure of O_{2g} [27]. SO₃ thus released into the atmosphere diffuses and dissolves in the Al₂O₃ scale, forming Al₂(SO₄)₃ as confirmed by XRD (Figure 4).

The sulphate particles in this scale combine with the oxide matrix in the reaction over long periods. According to the Gibbs free energy ($\Delta G_{700} = -807$ kJ) given in table 1, the chemical reaction is spontaneous when sulphur ions dissolved in the aluminium oxide matrix Al₂(SO₄)₃ diffuse into Al₂O₃ via Al³⁺ vacancy defects, eventually coming into contact with Al ions diffusing from the aluminide layer.

When the activities of both ions were high enough [5], Al₂S₃ forms as shown in the XRD results in Figure 4. This result supports the hypothesis that Na₂SO₄ decomposition supplies S for the direct formation of trace amounts of Al₂S₃ in the oxide scale at low temperatures (such as during Na₂SO₄ melting). EDS examination of the surface of the corroded sample (Figure 6c) showed the composition in wt% in which Fe (28.17 wt%) was higher than that of Al (13.65 wt%).

The composition of Al decreased because Al atoms diffused outwards to react first with oxygen, forming the Al₂O₃ scale and then diffused inwards into the steel substrate. Consequently, Al activity was decreased to a lower concentration, and the rest of the

Fe reacted with the rest of the Sg remaining in the atmosphere. This result explains why SO₃g and O₂g in the atmosphere also diffused into the aluminide layer to form FeSO₄ in which the Fe atom activity was high.

The low-formation energy of FeSO₄ ($\Delta G_{700} = -7.2 \text{ kJ}$) facilitated FeSO₄ dissociation to Fe₂O₃ and subsequent release of SO₂ into the atmosphere. The reaction of sulphur gas (as SO₂) with O₂g in the atmosphere also produced SO₃ gas. These reactions continued cyclically, forming an Fe-rich oxide (figure 6c) and Al₂S₃ as confirmed by XRD measurements (figure 4).

Consequently, Al₂O₃ failed to protect the aluminide layer and the steel substrate at 700°C during corrosion over long periods. 4. Conclusions The presence of NaCl and Na₂SO₄ deposits on the surface of AISI 1020 steel can accelerate oxidation and corrosion. However, the aluminizing coating on the steel could cause a one to three orders of magnitude reduction in k_p for oxidation at 700°C for 49 h in an environment containing Cl₂g and Sg, relative to that of steel without the coating. During the early stages of hot corrosion, a thin and dense Al₂O₃ scale was created.

During the subsequent corrosion, this Al₂O₃ layer 11 Page 8 of 8 Bull. Mater. Sci. (2020) 43:11 facilitated the formation of a porous Fe₂O₃ scale on itself, which allowed Cl and S penetration into the aluminide layer and enhanced the corrosion kinetics.

Vaporization of Al₂Cl₃ and Fe₂Cl₃ is believed to strongly affect the corrosion kinetics of AS with NaCl deposits, contributing to the decrease in weight gain after oxidation for 9 h. In contrast, S from Na₂SO₄ decomposition degraded the protective Al₂Cl₃ scale, allowing S to easily penetrate the oxide scale and form Al₂S₃. The consequent and appreciable increase in the penetration depth of S appears to have resulted in the precipitation of sulphide particles and growth of Fe₂O₃.

Acknowledgements The authors thank the Ministry of Research, Technology, and Higher Education of the Republic of Indonesia for financial support via the Incentive Research System of National Innovation and the National Strategy Research grant under contract number 529/UN26/8/LPPM/2016–2017. References [1] Subhash K, Jayaganthan R and Prakash S 2010 Bull. Mater. Sci. 33299 [2] Safadoost A, Davoodi M and Mansoori S A A 2014 J. Nat. Gas Sci. Eng.

19 105 [3] Mishra N K and Mishra S B 2015 Bull. Mater. Sci. 38 1679 [4] Lindberg D, Niemi J, Engblom M, Yrjas P, Lauren T and Hupa M 2016 Fuel Process. Technol. 141285 [5] Badaruddin M, Risano A Y E, Wardono H and Asmi D 2017 AIP Conf. Proc. 1788 030066 [6] Sen M, Balasubramaniam R and Kumar A V R 2000 Bull. Mater. Sci. 23399 [7]

Liu H H, Cheng W J and Wang C J 2011 Appl. Surf. Sci. 257 10645 [8] Badaruddin M, Wang C J, Wardono H, Tarkono and Asmi D 2016 AIP Conf. Proc.

1711 040002 [9] Wang C J and Li C C 2004 Surf. Coat. Technol. 177–178 37 [10] Wang C J, Lee J W and Twu T H 2003 Surf. Coat. Technol. 163–164 37 [11] Bose S 2018 High-temperature corrosion in High temperature coating, chapter 5, 2nd edn (Butterworth-Heinemann: Elsevier) 74. <https://doi.org/10.1016/C2015-0-01316-8> [12] Yajiang L, Juan W, Yonglan Z and Holly X 2002 Bull. Mater. Sci. 25635 [13] Bouche K, Barbier F and Coulet A 1998 Mater. Sci. Eng.

A 249 167 [14] Pieraggi B 1987 Oxid. Met. 27 177 [15] Badaruddin M and Sugiyanto 2013 Adv. Mater. Res. 789 463 [16] Koech P K and Wang C J 2018 Oxid. Met. 90 713 [17] Shi L 1993 Oxid. Met. 40 197 [18] Cizak C, Popa I, Brossard J M, Monceau D and Chevalier S 2016 Corros. Sci. 110 91 [19] Yan Y F, Xu X Q, Zhou D Q, Wang H, Wu Y, Liu X J et al 2013 Corros. Sci.

77 202 [20] Speight J G 2002 Lange's handbook of chemistry 16th edn (New York: McGraw-Hill) [21] Godlewska E, Mitoraj M and Leszczynska K 2014 Corros. Sci. 78 63 [22] Knacke O, Kubaschewski O and Hesselmann K 1977 Thermo-chemical properties of inorganic substance (Berlin: Springer) 91. <https://doi.org/10.1007/978-3-662-02293-1> [23] Neumann G 1990 in Diffusion in solid metals and alloys, numerical data and functional relationships in science and technology H Mehrer (ed) (Springer-Verlag, Berlin) vol.

26, p 152 [24] Le Claire A D 1990 in Diffusion in solid metals and alloys, numerical data and functional relationship in science and technology H Mehrer (ed) (Springer-Verlag, Berlin) vol. 26, p 129 [25] Tsaur C C, Rock J C, Wang C J and Su Y H 2005 Mater. Chem. Phys. 89 445 [26] Buscaglia V, Nanni P and Bottino C 1990 Corros. Sci. 30 327 [27] Lee W H and Lin R Y 1999 Mater. Chem. Phys.

58 231

INTERNET SOURCES:

17% - <https://www.ias.ac.in/article/fulltext/boms/043/0011>

<1% - <https://pubs.acs.org/doi/full/10.1021/nn501836x>

<1% - <https://medworm.com/journal/catalysis-communications.xml>

<1% - https://en.wikipedia.org/wiki/User:Enviromet/Copper_in_heat_exchangers

<1% -

https://www.researchgate.net/profile/Subhash_Kamal/publication/225590834_High_tem

perature_cyclic_oxidation_and_hot_corrosion_behaviours_of_superalloys_at_900C/links/0fcd501a020445a53000000.pdf?inViewer=true&disableCoverPage=true&origin=publication_detail

<1% - <https://en.wikipedia.org/wiki/Aquafortis>

<1% - <https://www.ncbi.nlm.nih.gov/pmc/articles/PMC4917166/>

<1% - <http://ijabme.org/File/J06.pdf>

<1% -

https://www.researchgate.net/publication/277355159_Formation_of_intermetallic_coatings_by_electrospark_deposition_of_titanium_and_aluminum_on_a_steel_substrate

<1% - <https://www.sciencedirect.com/science/article/pii/S0257897205012211>

<1% -

https://www.researchgate.net/publication/335151037_Effects_of_Oxide_Ions_on_the_Electrodeposition_Process_of_Silicon_in_Molten_Fluorides

<1% - <https://nepis.epa.gov/Exe/ZyPURL.cgi?Dockkey=2000WUE0.TXT>

<1% - <https://core.ac.uk/display/54844540>

<1% -

<https://www.scribd.com/document/268912608/Materials-for-Advanced-Power-Engineering-2006>

<1% - <https://www.sciencedirect.com/science/article/pii/B9780815515005500082>

<1% - <https://www.sciencedirect.com/science/article/pii/S027288421830261X>

<1% -

https://www.researchgate.net/publication/313265032_High-temperature_oxidation_behavior_of_aluminized_AISI_4130_steel

<1% -

https://www.researchgate.net/publication/312053211_Hot-corrosion_of_AISI_1020_steel_in_a_molten_NaClNa2SO4_eutectic_at_700C

<1% - <https://www.sciencedirect.com/topics/engineering/kirkendall-effect>

<1% - http://2018.cimtec-congress.org/abstracts_symposium_ch

<1% - <https://www.science.gov/topicpages/s/salt+stress-induced+inhibition>

<1% -

https://www.researchgate.net/publication/236946981_Preparation_of_highly_efficient_Al-doped_ZnO_photocatalyst_by_combustion_synthesis

<1% - <https://www.sciencedirect.com/science/article/pii/0921509395033459>

<1% - <https://www.sciencedirect.com/science/article/pii/S0038092X19303846>

<1% -

https://www.researchgate.net/publication/331071792_Fabrication_of_Porous_Materials_by_Spark_Plasma_Sintering_A_Review

<1% -

https://www.researchgate.net/publication/248455033_Template_Formation_of_Magnesium_Aluminate_MgAl2O4_Spinel_Microplatelets_in_Molten_Salt

<1% - <https://www.sciencedirect.com/science/article/pii/S004060901200661X>

<1% - <https://epdf.pub/shreirs-corrosion-volume-1.html>

<1% - https://www.researchgate.net/publication/266757237_High_Temperature_Corrosion_under_Laboratory_Conditions_Simulating_Biomass-Firing_A_Comprehensive_Characterization_of_Corrosion_Products

<1% - <http://d-scholarship.pitt.edu/8381/>

<1% - <https://www.sciencedirect.com/science/article/pii/S0257897214000097>

<1% - <http://library.umac.mo/ebooks/b28050253.pdf>

<1% - <https://epdf.pub/sulfur-in-magmas-and-melts-its-importance-for-natural-and-technical-processes.html>

<1% - https://booksite.elsevier.com/9780120885305/exercises/02~Web_Supplement_8.6.pdf

<1% - https://www.researchgate.net/publication/280008278_An_overview_of_Na2SO4_ANDOR_V2O5_induced_hot_corrosion_of_Fe-_and_Ni-Based_superalloys

<1% - https://www.researchgate.net/publication/273289155_Optimizing_NiCr_and_FeCr_HVOF_Coating_Structures_for_High_Temperature_Corrosion_Protection_Applications

<1% - https://www.researchgate.net/publication/229387244_Microstructure_spallation_and_corrosion_of_plasma_sprayed_Al2O3-13TiO2_coatings

<1% - https://www.researchgate.net/publication/222624157_The_oxidation_of_Fe3Al-0_2_4_6Cr_alloys_at_1000C

<1% - https://www.researchgate.net/publication/283543513_Mutant_HRAS_as_novel_target_for_MEK_and_mTOR_inhibitors

<1% - <https://www.sciencedirect.com/science/article/pii/S0956053X17305354>

<1% - https://www.researchgate.net/publication/249551411_Sedimentary_dolomite_A_reality_check

<1% - <https://www.sciencedirect.com/science/article/pii/S0042207X04004786>

<1% - https://www.researchgate.net/publication/234018333_Oxidation_behaviour_of_Fe40Al_alloy_strip

<1% - https://www.researchgate.net/publication/222825825_Microstructural_investigation_of_the_breakdown_of_the_protective_oxide_scale_on_a_304_steel_in_the_presence_of_oxygen

n_and_water_vapour_at_600C

<1% - <https://onlinelibrary.wiley.com/doi/10.1111/bcpt.13266>